Indian Journal of Design Engineering (IJDE)
ISSN: 2582-8584 (Online), Volume-4 Issue-1, February, 2024

Integrated Crashworthiness Analysis of Electric Vehicle Battery Shells and Chassis: A Finite Element Study with Abaqus

Mizanur Rahman, Mahendher Marri, Abel Varghese

Abstract: ***This paper aims to comprehend and predict the mechanical behavior of the genuine Tesla Model-S chassis and the battery module during a crash in Abaqus/Explicit. The parametric method was incorporated with varying impact velocities from 27.7, 55.5, and 100m/s and battery shell thickness from 1mm to 3mm. The asymmetry model was considered for both the chassis and battery pack. Aluminum 6061 and ASI430 SS are assigned to the chassis profile and the battery shells (cells). A Johnson-Cook (JC) plastic and damage failure model has been implemented to simulate realistic crash behavior. Displacement, energy, and force results were captured during the simulation. A battery shell thickness of 3mm showed higher resistance than a 1mm thick shell at 55.5 m/s. The numerical findings reveal the dynamic response in displacement and compression under various loading conditions for both individual profiles. Additionally, the study presents a detailed inspection of each cell module, graphically demonstrating how the individual cells respond to initial positions, crashes, and external deformation (shear) caused by collision energy. The finite element model is validated against previous experimental and numerical studies, successfully simulating crashworthiness. The present study provides significant insights that have the potential to improve the safety and efficiency of battery-operated vehicles through the design and optimization of their structures.***

Keywords: ***Abaqus/Explicit, Crashworthiness, Dynamic Impact, Electric Vehicle.***

Nomenclature

U – Displacement, mm
EV - Electric vehicle
σ - Equivalent stress, pa
n - Hardening coefficient
HV - Hybrid vehicle
JC - Johnson-cook
LIB - Lithium-ion batteries
σ_m – Mean stress, pa
T_m – Melting temperature, K
ε_f - Plastic fracture strain
RF - Reaction Force, kN
T_r – Room temperature, K
m – Softening coefficient
$\dot{\varepsilon}^*$ - Strain rate
ε - True strain
v – Velocity, m/s

Manuscript received on 01 February 2024 | Revised Manuscript received on 10 February 2024 | Manuscript Accepted on 15 February 2024 | Manuscript published on 30 May 2024.
**Correspondence Author(s)*
Mizanur Rahman, School of Engineering and Physical Sciences, Heriot-Watt University, Edinburgh EH14 4AS, UK.
Mahendher Marri*, School of Engineering and Physical Sciences, Heriot-Watt University, Edinburgh EH14 4AS, UK. E-mail: mahendher.marri1@gmail.com, ORCID ID: 0000-0002-4532-3722
Abel Varghese, School of Engineering and Physical Sciences, Heriot-Watt University, Edinburgh EH14 4AS, UK.

I. INTRODUCTION

The future of automotive transposing into electric vehicles is beyond agreement. Before these battery-powered vehicles leave the factory, they must meet a similar safety standard to conventional vehicles. Lithium batteries were used to power electric vehcles (EVs) because of their nature of having higher energy density, voltage capacity, and a slow self-discharge rate [1]. Fig 1 ([2]) represents the bare Tesla chassis. These batteries were protected by layers of other vehicle components, such as doors, chassis, and carbon fiber epoxy [3]. The vehicle's secondary safety classification describes protecting the vehicle and passengers during a crash [4]. The safety measures of EVs are different from gas-powered vehicles. These questions challenge automakers to ensure and improve the degree of safety of the occupants during any traffic incidents. These can be translated into the safety hazard of EV drives: the high possibility of internal short-circuit, overheating, fire safety, explosion, and chemical acid risk [5, 6]. Therefore, the various essential test practices are required to set an appropriate stage of safety. Aluminum alloy is extensively used due to its characteristics of corrosion resistance, weldability, and high toughness value [7]. The primary role of an automotive vehicle is to transport citizens from one place to another comfortably and safely, with the occupant's safety risk discussed above for EVs. This ideology was developed when Tesla introduced a new battery design with a 3mm thickness, replacing their previous models.

Fig. 1. Tesla Model-S Chassis with Batteries and Motors [2]

II. LITERATURE STUDY

A. Li-ion Battery Shell in EV

In 1873, Davidson introduced the first fuel vehicle in 1885. The luxury trend peaked significantly as the USA enforced the Research Development and Demonstration Act EVs and Hybrid Vehicles (HV) [8]. Currently, each automobile supplier produces either EV or HV on their productions. Furthermore, Toyota found remarkable success with the first hybrid electric vehicle (HEV) in the late 1990s, on their model Toyota Prius, operating with low energy density batteries, the Ni-Cd Hydride [9]. The mechanical behavior of battery cells of EVs under crash performance has lately drawn global attention [10, 11]. Kisters et al. [12] found that Li-ion cells adjust significantly over different speeds, as per the impact test. Xu et al. [13] studied and implemented an experiment on the batteries to understand the failure of the LIB's electrodes.

Furthermore, the test also discovered the plastic and fracture properties of the cylinder shell, which failed the quasi-static loading. EV crashworthiness analysis design requires an equivalent homogenized battery pack [14-16][38][39][40]. Lai et al. [17] observed additional mechanical behavior on LIB during crashworthiness. The buckling kink and shear band formation and the final densification of the LIB cell describe the cell's representative volume element. However, the present investigations do not contemplate the thermal behavior of the battery cell structure.

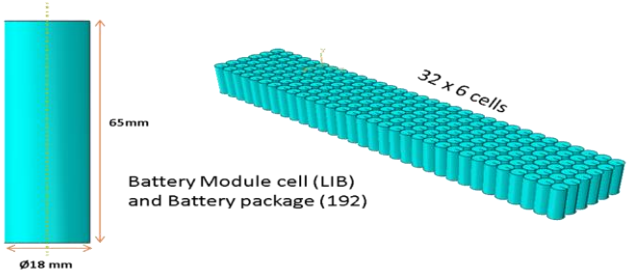

Fig. 2. Shows the Geometrical Dimensions of the Battery Shell and Stacked Batteries

Fig. 3. (a) Represents the Tesla Models-S Assembled Battery Pack and (b) Individual Pack [31]

B. EV Aluminum Alloy Chassis

The chassis provides the primary protection for the battery packs during high-velocity collision. It is essential to evaluate different types of materials while manufacturing structures for vehicles, which can absorb and transform kinetic energy into elastic strain energy, heat energy, and fracture energy at the crash zone [18-20]. Aluminum alloy is well-known and widely used in aerospace, automobiles, and rail transportation because of its high strength in a medium application, resistance to corrosion, heat treatability, weldability, and structural lightness [21]. In 2006, the usage of aluminum overtook cast iron as the second-highest material in North American vehicles [22]. Among most aluminum alloys, the 6000 series (AA6061) aluminum is commonly used by automotive manufacturers. In order to maximize the effective range of EVs, engineers had to adapt lightweight materials as much as possible; compared with other materials such as steel, aluminum aims to provide 28% in a vehicle's weight reduction [20]. These also increase fuel efficiency and successively lower harmful carbon emissions into the environment [23]. Researchers examined the aluminum alloy chassis at different impact loading conditions, and to simulate the experimental data, Lemaitre, Gologanu, Gurson, and JC damage models [24, 25] were implemented to achieve the physical-based results. The importance of these models is to investigate the mechanical properties of materials in impact problems. The well-known and undertaken model is Johnson Cook, which characterizes the material behavior in stress response at considerable strain rates and elevated temperatures. Lin et al. [26] have provided a more effective, accurate, and precise approximation of the flow stress for the standard high-strength alloy steel by combining JC and Zerilli-Armstrong (ZA). The standardized Charpy impact test is a low-budget test that is also reliable, and the test proposes to measure the toughness of material under impact loading at a multi-axial stress rate [18]. Hufenbach et al. [27] studied the resistance of composite materials under impact loading. Peng et al. [28] examined a similar Charpy impact test approach for energy-absorbing structures withAA6082-T6 material. Two group tests have been performed to maintain the specimens' size and vary the notch depth, and these two tests have been developed in finite elements. The simulation presented an agreeable result of 16.34% for FEA and 24.38% for the experiment [25].

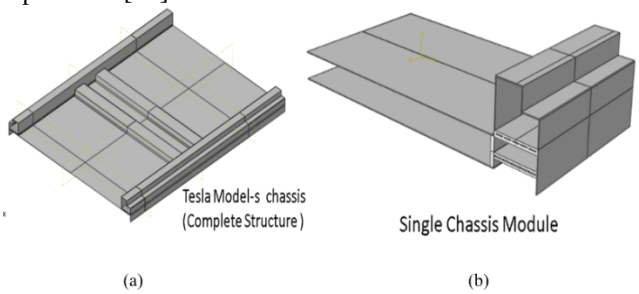

Fig. 4. (a) CAD model of Tesla Model S Chassis and (b) Symmetry Model of Chassis

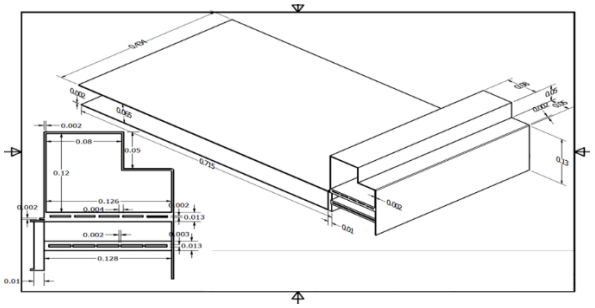

Fig. 5. Illustrates the Geometrical Dimensions of the Tesla Model S Chassis

III. NUMERICAL MODELS

A. Model Material Properties

The JC plasticity and damage model is well-known for material failure response following large deformations, high strain rates, and temperatures. In the present study, these JC equations are considered to investigate the mechanical behavior of selected materials under impact simulations. The flow stress can be denoted as [17, 24, 25, 29, 30],

$$\sigma = [A + B\varepsilon^n][1 + Cln\dot{\varepsilon}^*][1 - (T^*)^m] \quad (1)$$

Where σ represents the equivalent stress, ε is the true strain, $\dot{\varepsilon}^*$ equivalent strain rate, A, B, C are individual material parameters which are determined with the help of tensile testing, n refers to the hardening coefficient and where m is softening exponents. T^* is expressed as $T^* = (T - T_r)/(T_m - T_r)$, where T_r is the room temperature and T_m melting temperature. In association with fracture deformation of metals, a JC damage failure model is relevant to high-strain rates under dynamic conditions. The progressive damage and failure models are advised for other investigations, such as quasi-static procedures where the demand for element removal is necessary for Gurson plasticity. The expression given by the Johnson-Cook dynamic failure model is denoted as:

$$\varepsilon_f = \left[D_1 + D_2 exp\left(D_3\left(\frac{\sigma_m}{\sigma_{eq}}\right)\right)\right][1 + D_4 ln(\dot{\varepsilon_p}^*)][1 + D_5 T^*] \quad (2)$$

Where ε_f is the equivalent plastic fracture strain, associated with strain rate and temperature in addition to stress triaxiality, σ_m is the mean stress and σ_{eq} is the equivalent of stress. D_1, D_2, D_3, D_4, D_5 are material constants determined from various strain tests shown in Table 3.

B. Simulation Setup

A CAD model was developed using Autodesk Inventor 2022 and later imported into Abaqus/Explicit. It was the initial methodology for the present numerical analysis; however, the finite element analysis is carried out under an educational license. Therefore, Abaqus is limited in performing many elements; a single module has been constructed in Fig 4 (a, b) and Fig 5 shows the blueprint of the symmetric chassis. External supportive enforcement, such as doors and other materials, were excluded in the current study. The Tesla battery module had 16 modules, as shown in Fig 3 (a, b) [31]. The Geometry of individual LIB-cells is adapted from previous studies [30, 32] with a height of 65mm and diameter of 18mm with alerting shell thickness between 3 and 1mm. Fig 2 shows the current battery pack simulation setup, which consists of 192 individual cells. The dimensions of the model and its components are hand-measured from the assembly of the Tesla Model-S chassis [2]. The chassis and battery shells were assembled with symmetry conditions to reduce computational cost. For Li-ion battery shell ASI 430 SS [33] and chassis aluminum, 6061 [18] were assigned. Table 1-3 consists of the mechanical properties of various aluminum alloys and steels [18, 29, 33-35]. The entire setup, including the chassis and battery packs, is assembled with tie-constrained interaction, as shown in Fig 6. Every cell is in contact with four neighboring cells, apart from the one outer side of the module. A coefficient of friction of 0.1 was defined between battery shells and chassis.

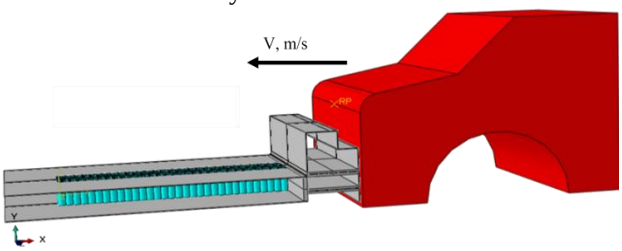

Fig. 6. Assembly set up in Abaqus/explicit and red Defines the Impactor (Analytical Rigid Car Model)

Table 1. Johnson Cook Plasticity Parameters for Battery Shell

Material	A [Mpa]	B [Mpa]	c	n	m	$T_{melting}, K$	$\dot{\varepsilon}$	E [Gpa]	ϑ
ASI 430 Stainless steel [33]	349.6	307.9	0.062	0.3478	0.919	1425	1	200	0.3
Steel 4340 [34]	792	510	0.14	0.26	1.03	1793	1	200	0.29
AMRCO IRON [34]	175	380	0.06	0.32	0.55	1811	1	207	0.29
OFHC COPPER [34]	90	292	0.025	0.31	1.09	1356	1	124	0.34

Table 2. Johnson Cook Plasticity Parameters for Chassis

Material	A, [Mpa]	B, [Mpa]	c	n	m	$T_{melting}, K$	$\dot{\varepsilon}$	E, [Gpa]	ϑ
Aluminum 6061-T6 [18]	324	114	0.002	0.42	1.34	925	1	69	0.32
AA6082-T6 [35]	201.55	250.87	0.0097	0.206	1.31	855	0.001	70	0.3
Aluminum 7075-T6 [29]	473	210	0.033	0.381	-	-	0.001	-	-

Table 3. Johnson Cook Damage Parameters for Chassis

d_1	d_2	d_3	d_4	d_5	Ref
-0.77	1.45	-0.47	0	1.6	[18]

The dynamic step was created with a time of 0.001s. The chassis and battery shell were meshed with C3D8R (Continuum 3D 8-node reduced integration) and S4R (shell 4 nodes reduced integration), resulting in 214,662 elements. The impactor was modelled using analytical rigid, close to a real car and does not require mesh to simulate. Creating boundaries and conditions varies from deformable bodies. Rigid bodies require a point (reference point) to assign conditions and can be created anywhere on the body. In this case, a mass of approx.2200kg (shared by the Tesla sales team at the time of the visit to the showroom), equal to a Tesla car [2], was assigned to a rigid body.

Table 4 consists of the initial and residual (impacted) velocities for rigid impactor. All DOFs are enabled for battery shells to capture the displacements caused by impact simulation. The following section describes the simulated model's validation with various published experiments and simulation data. Moreover, ±2 % of human error was considered in manual measuring dimensions.

Table 4. Simulation velocity setup for rigid impactor.

Initial Velocities		
km/h	**m/s**	**Impacted Velocity, m/s**
100	27.77	26.99
200	55.5	54.76
360	100	92.7

IV. RESULTS AND DISCUSSION

A. Validation of Numerical Simulation

Selected material for the Tesla chassis is simulated and validated with dynamic axial crushing from [36]. Axial compression is divided into static and dynamic categories on AA circular tubes. Current FE results are compared with experimental data of DRA 11 samples. Two-step verification has been implemented: 1) to study the force and energy absorbed by the chassis and 2) to study the material deformation of the chassis. Simulated results showed an excellent cure fit with published data, as shown in Fig 7 [36]. Al6061 – T6 experienced ~16mm displacement compared to Al6060 (experiment and simulation) under 120kN. Due to mechanical properties like plasticity and elastic limit, they are lower than Al6061. However, regarding durability and light structure, the Al6061-T6 stands out. Fig 8 compares the experiment and current simulation, which achieved approx. 5 folding and error between 2-17%. Later, static analysis was executed on a stainless steel (SS) battery shell with a rigid analytical indenter and using identical load conditions [36]. The end caps of the shell are encastred (left and right). Surface-to-surface contact interaction is assigned between the rigid impactor and the peripheral of the battery shell, allowing 1DoF to the impactor. Fig 9 shows the indentation of the SS battery shell and achieves a similar indentation depth to [36]. However, many other factors may affect the deformation of Li-ion batteries, like short circuits, chemical reactions, etc.

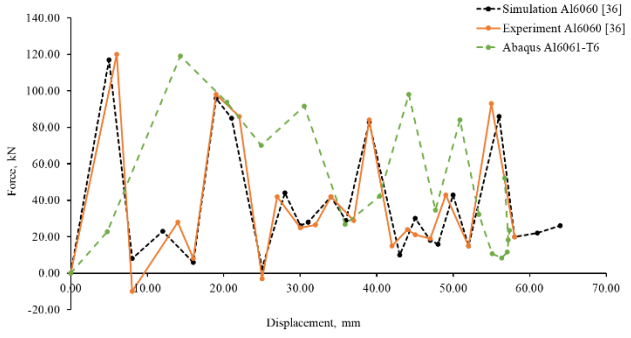

Fig. 7. Shows the Validation of the Currently Selected Material (Abaqus Al6061-T6) with Published Data

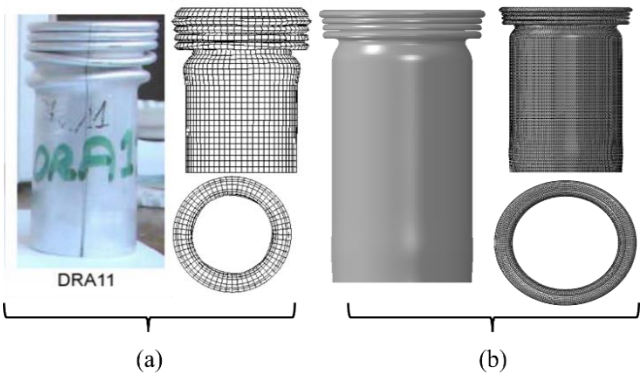

Fig. 8. Photographic Comparison of Battery Material (a) Axial Compression of Experiment and Simulation from [36]. (b) Current Compression Simulation

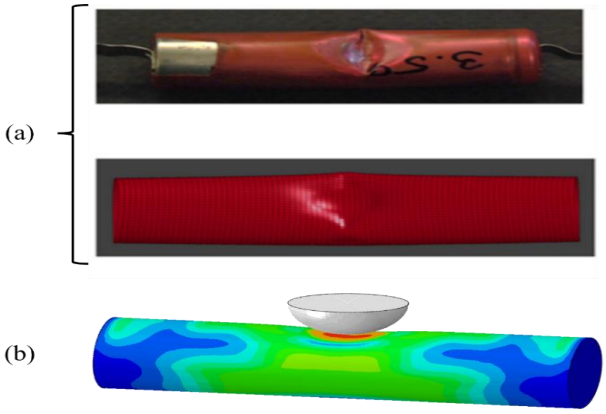

Fig. 9. Photographic Comparison of Battery Material (a) Indentation of Experiment and Simulation from [36]. (b) Current Simulation on Li-ion

B. Simulation Results

A crashworthiness simulation was conducted on the Tesla Model S in Abaqus/Explicit. Five parametric simulations have been carried out in this project, varying impact velocities from 27.7, 55.5, and 100 m/s with the changing thickness of lithium-ion battery shell casing from 1 and 3mm. 18 simulations were carried out successfully using 8-core CPU machines. Fig 10 shows the summaries of all parametric simulation results. High displacement (deformation) is seen in the chassis compared to battery shells. The reason can be that the chassis guarded the battery module, which is the first place of contact in this analysis. Fig 12 compares the battery shell with 1 and 3mm thickness and chassis for an impact velocity of 27.7m/s. A significant variation was achieved between the 1mm and 3mm battery shell, resulting in higher RF with minimal displacement than 1mm.

Moreover, a 1mm shell occurred steadily around 19.6mm and a 3mm shell after 29mm. Likewise, chassis performance perceived equivalent outcomes as battery module. The deformation of shells is minimal for 27.7 m/s compared to 55.5 or 100 m/s.

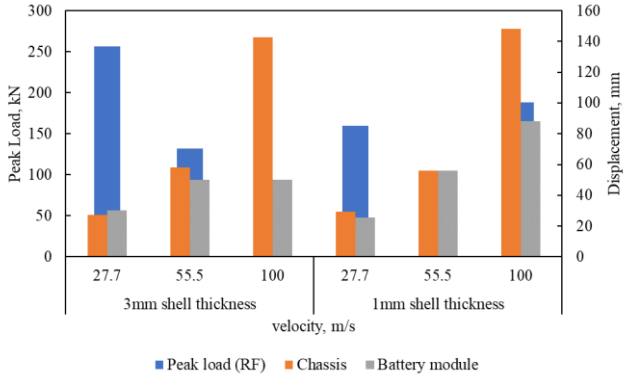

Fig. 10 Represents the Summarised Results of all Configurations with Battery Module and Chassis Assembly

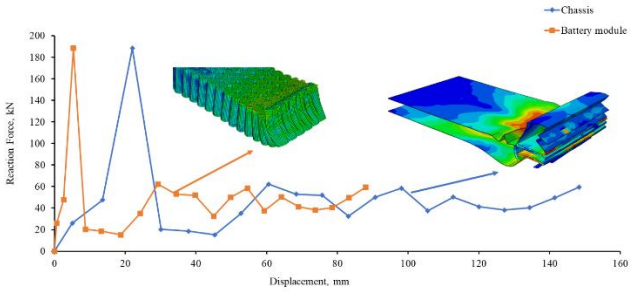

Fig. 11 Comparison of Reaction Force and Displacement for 1mm Shell Thickness at 100m/s Impact Velocity

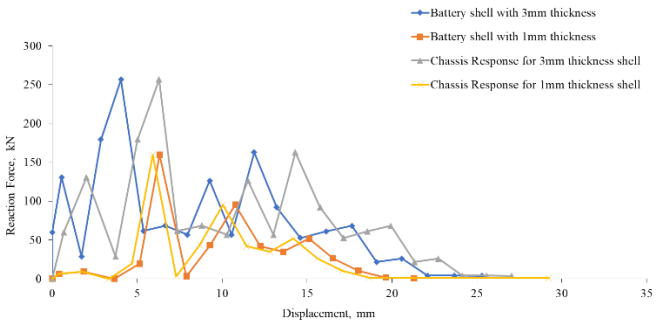

Fig. 12 Comparison of Reaction Force and Displacement for 1mm and 3mm Shell Thickness at 27.7m/s Impact Velocity

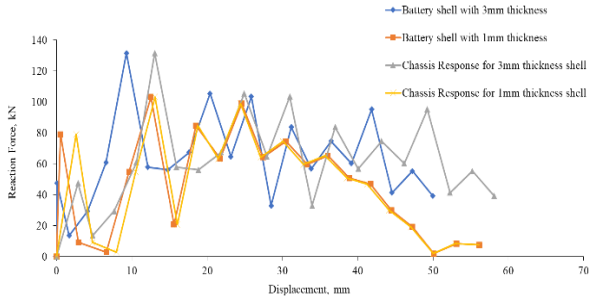

Fig. 13 Comparison of Reaction Force and Displacement for 1mm and 3mm Shell Thickness at 55.5m/s Impact Velocity.

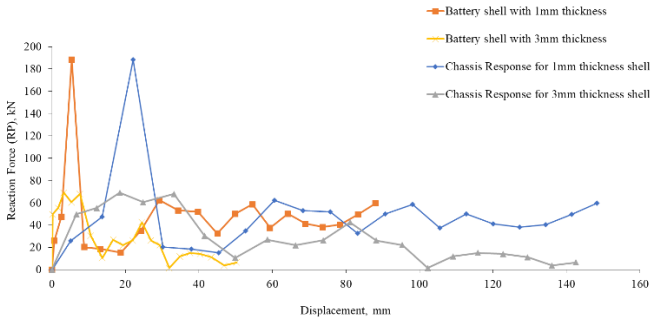

Fig. 14 Comparison of Reaction Force and Displacement for 1mm and 3mm Shell Thickness at 100m/s Impact Velocity

On the other hand, impact velocity changed from 27.7m/s to 55.5m/s (200km/h) with similar conditions in Fig 13. For 55.5m/s, impact velocity 1mm thick shell showed minor displacement compared to 27.7m/s. A good relationship was shown between the chassis and the battery after 18mm displacement (under 75kN RF). It caused a drastic drop in RF from 256kN to 131kN for 27.7m/s and 55.5m/s, respectively. Approx. 15.5% decrease in RF for 1mm thick subjected to 55.5m/s against 27.7m/s. Dealignment occurred in both modelling modes (thickness), illustrated in Fig 17. A close agreement appeared among batteries and chassis relative to impact positions.

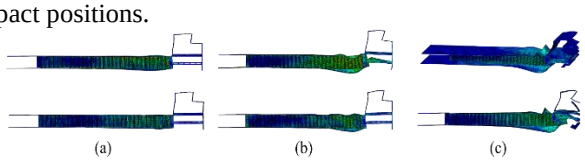

Fig. 15 Post-Processed Results (Side View) of the Battery Module and Chassis at Various Velocities. The First and Second Rows Have Shell Thicknesses of 3mm and 1mm, Respectively. Impact Velocities are as Follows: (a) at 27.7m/s, (b) 55.5m/s, and (c) 100m/s

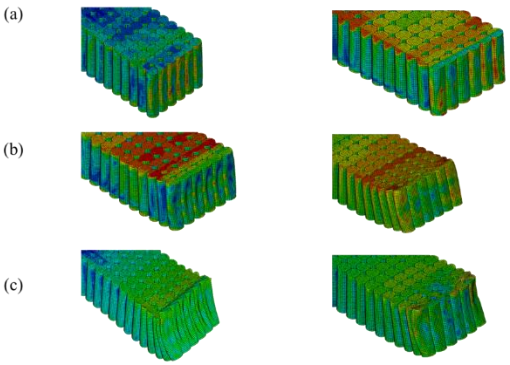

Fig. 16 Shows the Front Rows of the Battery Module During Impact Simulation. (a) at 27.7m/s for 1mm (Left side) and 3mm (Right Side), (b) at 55.5m/s for 1mm (Left side) and 3mm (Right Side), and (c) at 100m/s for 1mm (Left Side) and 3mm (Right Side)

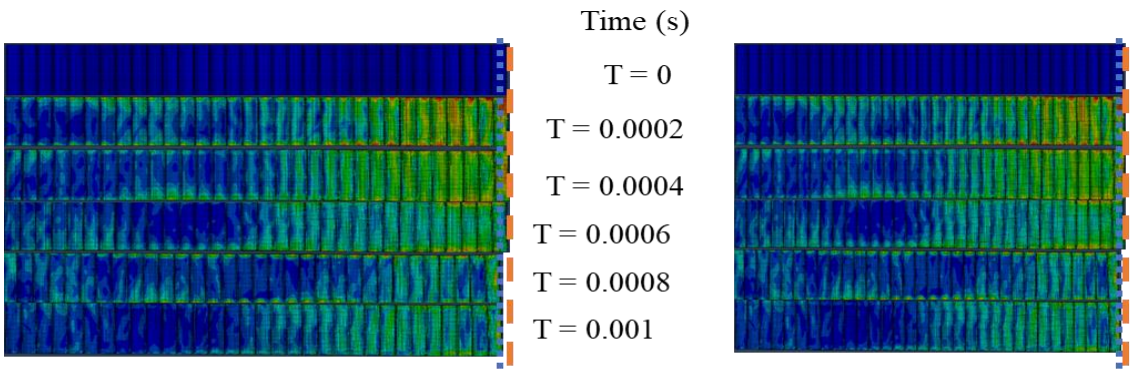

Deformation of battery module with 1mm (left side) and 3mm (right side) shell thickness at 27.7m/s

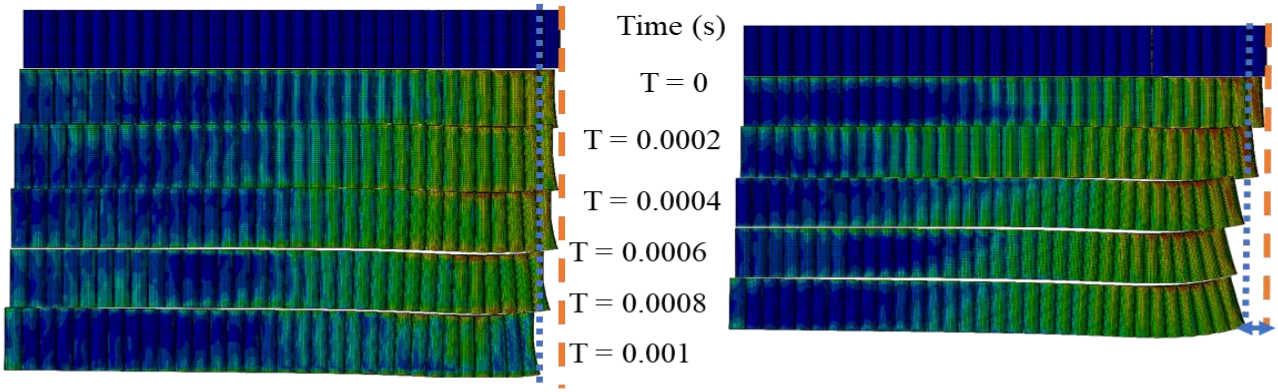

Deformation of battery module with 1mm (left side) and 3mm (right side) shell thickness at 55.5m/s

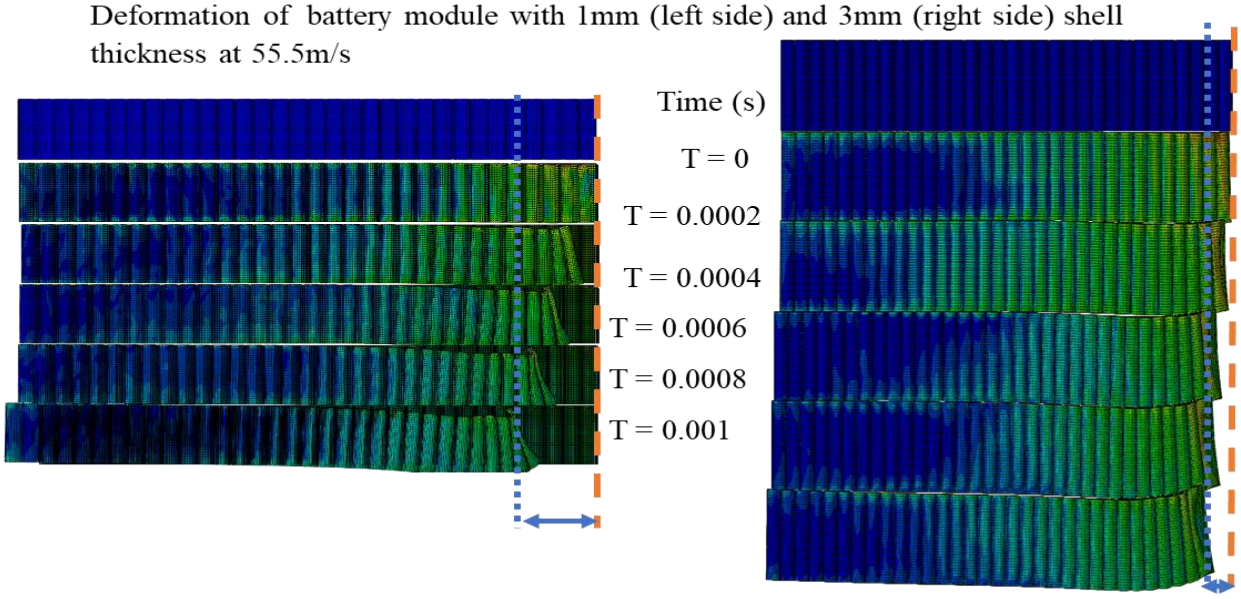

Deformation of battery module with 1mm (left side) and 3mm (right side) shell thickness at 100m/s

Deformed ..... Initial — — — —

Fig. 17 Represents the Photographic Representation of the Battery Module (Excluding Chassis) at Time Increments

Figures 11 and 14 illustrate the comparison of the chassis and battery module (with 1mm and 3mm shell thickness, respectively) for an impact velocity of 100 m/s. There were overshoots in the chassis and battery module, approx.—23mm and approx.—5.5mm, respectively, achieved at the same reaction force ~189kN. An identical result was evolved in a previously published paper [37] on the bottom surface of the battery using two various indenters. The reasons for overshooting batteries are modelled with an empty casing, and the front end of the chassis has two support beams, which involved nearly 70% damage as per the simulation assembly.

Figs. 15 (a, b, c) and 16 illustrate separating the assembly's frontal part and contact area. The displacement of the 1mm battery shell and 3mm chassis response is almost equal with a variation of forces. In contrast, this 3mm battery shell presented a closure agreement with a 1mm thick shell after ~25mm in displacement. After 30mm displacement, the chassis and battery module presented lower reaction force (RF), and the kinetic energy in the impactor may be fully or semi-transferred to the chassis with significant chassis deformation. These results show that increasing shell and chassis thickness can absorb or reduce deformation. Due to this, front-row cells are dismantled from the assembly and contribute to the penetration of the top surface of the chassis shown in Fig 15 (a, b, c).

V. CONCLUSION

In summary, this study uses Abaqus/Explicit to explore the mechanical dynamics of the Tesla Model-S chassis and battery module during a crash. The study's practical application is improved by including an asymmetry model for the battery pack and chassis and using ASI430 SS and Aluminum 6061 components. The precise simulation of crash behavior is made possible by applying a damage failure model and a Johnson-Cook plasticity model. Notably, at 55.5 m/s, the observed resistance variations between battery shell thicknesses provide insightful information that can be applied to optimising structures in different battery-operated vehicles, reducing the chance of failure. The simulation results demonstrated the mechanical behavior of the material under dynamic impact response: Peak load, Reaction force-displacement, deformation, deformation dealignment altering shell casing thickness of Li-ion, and different velocity profiles. Derived conclusions as follows,

1. The numerical findings demonstrated the dynamic response in displacement and compression under various loading conditions of both individual profiles.
2. In all configuration setups, the lower velocity profile from 55.m/s with 3mm shell casing responded with higher resistive force than a thickness of 1mm.
3. High speed resulted in significant displacement for chassis profile in both 3mm and 1mm thickness of shell casing. However, in the case of shell casing with a hypervelocity of 100 m/s, the distinction between 3mm to 1mm thickness is significantly lower.
4. The present research goes a step further by explaining and graphically presenting a detailed inspection of each cell module, showing how the individual cells will respond from their initial positions, crash, and be externally deformed (shear) by collision energy.
5. The finite element model is validated with previous experimental and numerical studies and successfully simulated to visualize crashworthiness.

ACKNOWLEDGEMENT

The authors would like to thank the Tesla Motors sales team in Dubai, United Arab Emirates, who accepted our request to visit and permitted us to have a close view and take measurements of the Model S chassis.

DECLARATION STATEMENT

Funding	No, I did not receive.
Conflicts of Interest	No conflicts of interest to the best of our knowledge.
Ethical Approval and Consent to Participate	No, the article does not require ethical approval and consent to participate with evidence.
Availability of Data and Material	Not relevant.
Authors Contributions	All authors have equal participation in this article.

REFERENCES

1. R. Teki *et al.*, "Nanostructured Silicon Anodes for Lithium Ion Rechargeable Batteries," *Small*, vol. 5, no. 20, pp. 2236-2242, 2009/10/16 2009, doi: https://doi.org/10.1002/smll.200900382.
2. Tesla. "Tesla." Tesla. https://www.tesla.com/en_ae (accessed January, 2021).
3. R. Garg *et al.*, "Predicting composite component behavior using element level crashworthiness tests, finite element analysis and automated parametric identification," *Materials*, vol. 13, no. 20, p. 4501, 2020. https://doi.org/10.3390/ma13204501
4. J. Broughton, "The benefits of improved car secondary safety," *Accident Analysis & Prevention*, vol. 35, no. 4, pp. 527-535, 2003. https://doi.org/10.1016/S0001-4575(02)00030-1
5. J. Xu, Y. Wu, and S. Yin, "Investigation of effects of design parameters on the internal short-circuit in cylindrical lithium-ion batteries," *RSC advances*, vol. 7, no. 24, pp. 14360-14371, 2017. https://doi.org/10.1039/C6RA27892B
6. K. Davidsson, I. Karlsson, P. Leisner, M. Bobert, and P. Blomqvist, "Safety test methods for EV batteries," *World Electric Vehicle Journal*, vol. 4, no. 2, pp. 414-420, 2010. https://doi.org/10.3390/wevj4020414
7. K. Buchanan, K. Colas, J. Ribis, A. Lopez, and J. Garnier, "Analysis of the metastable precipitates in peak-hardness aged Al-Mg-Si (-Cu) alloys with differing Si contents," *Acta Materialia*, vol. 132, pp. 209-221, 2017. https://doi.org/10.1016/j.actamat.2017.04.037
8. K. T. Chau, Y. S. Wong, and C. C. Chan, "An overview of energy sources for electric vehicles," *Energy Conversion and Management*, vol. 40, no. 10, pp. 1021-1039, 1999. https://doi.org/10.1016/S0196-8904(99)00021-7
9. M. Li, J. Lu, Z. Chen, and K. Amine, "30 years of lithium-ion batteries," *Advanced Materials*, vol. 30, no. 33, p. 1800561, 2018. https://doi.org/10.1002/adma.201800561
10. X. Hu, J. Jiang, D. Cao, and B. Egardt, "Battery health prognosis for electric vehicles using sample entropy and sparse Bayesian predictive modeling," *IEEE Transactions on Industrial Electronics*, vol. 63, no. 4, pp. 2645-2656, 2015.
11. E. Karden, S. Ploumen, B. Fricke, T. Miller, and K. Snyder, "Energy storage devices for future hybrid electric vehicles," *Journal of Power Sources*, vol. 168, no. 1, pp. 2-11, 2007. https://doi.org/10.1016/j.jpowsour.2006.10.090
12. T. Kisters, E. Sahraei, and T. Wierzbicki, "Dynamic impact tests on lithium-ion cells," *International Journal of Impact Engineering*, vol. 108, pp. 205-216, 2017. https://doi.org/10.1016/j.ijimpeng.2017.04.025
13. J. Xu, B. Liu, and D. Hu, "State of charge dependent mechanical integrity behavior of 18650 lithium-ion batteries," *Scientific reports*, vol. 6, no. 1, p. 21829, 2016. https://doi.org/10.1038/srep21829
14. E. Sahraei, T. Wierzbicki, R. Hill, and M. Luo, "Crash safety of lithium-ion batteries towards development of a computational model'," *Electric and Hybrid-Electric Vehicles–Batteries*, p. 31, 2010. https://doi.org/10.4271/2010-01-1078
15. J. Xu, B. Liu, X. Wang, and D. Hu, "Computational model of 18650 lithium-ion battery with coupled strain rate and SOC dependencies," *Applied Energy*, vol. 172, pp. 180-189, 2016. https://doi.org/10.1016/j.apenergy.2016.03.108
16. T. Wierzbicki and E. Sahraei, "Homogenized mechanical properties for the jellyroll of cylindrical Lithium-ion cells," *Journal of power sources*, vol. 241, pp. 467-476, 2013. https://doi.org/10.1016/j.jpowsour.2013.04.135

17. W.-J. Lai, M. Y. Ali, and J. Pan, "Mechanical behavior of representative volume elements of lithium-ion battery cells under compressive loading conditions," *Journal of Power Sources*, vol. 245, pp. 609-623, 2014. https://doi.org/10.1016/j.jpowsour.2013.06.134
18. S. Pervaiz, S. Kannan, K. Ram, and W. A. Samad, "Numerical modeling of Charpy impact test to determine the fracture characteristics of aluminium alloy 6061," 2019: Springer, pp. 85-88. https://doi.org/10.1007/978-3-319-95879-8_14
19. I. Guzmán, E. Granda, B. Vargas, C. Cruz, Y. Avila, and J. Acevedo, "Tensile and fracture behavior in 6061-T6 and 6061-T4 aluminum alloys welded by pulsed metal transfer GMAW," *The International Journal of Advanced Manufacturing Technology*, vol. 103, pp. 2553-2562, 2019. https://doi.org/10.1007/s00170-019-03673-7
20. B. Simhachalam, K. Srinivas, and C. L. Rao, "Energy absorption characteristics of aluminium alloy AA7XXX and AA6061 tubes subjected to static and dynamic axial load," *International Journal of Crashworthiness*, vol. 19, no. 2, pp. 139-152, 2014. https://doi.org/10.1080/13588265.2013.878974
21. J. C. Benedyk, "Aluminum alloys for lightweight automotive structures," in *Materials, design and manufacturing for lightweight vehicles*: Elsevier, 2010, pp. 79-113. https://doi.org/10.1533/9781845697822.1.79
22. J. C. Benedyk, "3 - Aluminum alloys for lightweight automotive structures," in *Materials, Design and Manufacturing for Lightweight Vehicles*, P. K. Mallick Ed.: Woodhead Publishing, 2010, pp. 79-113. https://doi.org/10.1533/9781845697822.1.79
23. S. Wenlong, C. Xiaokai, and W. Lu, "Analysis of energy saving and emission reduction of vehicles using light weight materials," *Energy Procedia*, vol. 88, pp. 889-893, 2016. https://doi.org/10.1016/j.egypro.2016.06.106
24. H.-Y. Che, L. Zhu, D.-Z. Sun, J.-H. Chen, and H. Zhu, "Characterization and modeling of aluminum extrusion damage under crash loading," *Thin-walled structures*, vol. 45, no. 4, pp. 383-392, 2007. https://doi.org/10.1016/j.tws.2007.04.004
25. X. Chen, Y. Peng, S. Peng, S. Yao, C. Chen, and P. Xu, "Flow and fracture behavior of aluminum alloy 6082-T6 at different tensile strain rates and triaxialities," *PloS one*, vol. 12, no. 7, p. e0181983, 2017, doi: 10.1371/journal.pone.0181983. https://doi.org/10.1371/journal.pone.0181983
26. Y. C. Lin, X.-M. Chen, and G. Liu, "A modified Johnson–Cook model for tensile behaviors of typical high-strength alloy steel," *Materials Science and Engineering: A*, vol. 527, no. 26, pp. 6980-6986, 2010. https://doi.org/10.1016/j.msea.2010.07.061
27. W. Hufenbach, F. M. Ibraim, A. Langkamp, R. Böhm, and A. Hornig, "Charpy impact tests on composite structures–an experimental and numerical investigation," *Composites Science and Technology*, vol. 68, no. 12, pp. 2391-2400, 2008. https://doi.org/10.1016/j.compscitech.2007.10.008
28. Y. Peng, W. Deng, P. Xu, and S. Yao, "Study on the collision performance of a composite energy-absorbing structure for subway vehicles," *Thin-Walled Structures*, vol. 94, pp. 663-672, 2015. https://doi.org/10.1016/j.tws.2015.05.016
29. D.-N. Zhang, Q.-Q. Shangguan, C.-J. Xie, and F. Liu, "A modified Johnson–Cook model of dynamic tensile behaviors for 7075-T6 aluminum alloy," *Journal of Alloys and Compounds*, vol. 619, pp. 186-194, 2015. https://doi.org/10.1016/j.jallcom.2014.09.002
30. L. Tang, J. Zhang, and P. Cheng, "Homogenized modeling methodology for 18650 lithium-ion battery module under large deformation," *Plos one*, vol. 12, no. 7, p. e0181882, 2017. https://doi.org/10.1371/journal.pone.0181882
31. M. U. Cuma, E. Yirik, Ç. Dericioğlu, E. Ünal, B. Onur, and M. Tumay, "Design considerations of high voltage battery packs for electric buses," *Int. J. Adv. Automot. Technol*, vol. 1, no. 2, pp. 73-79, 2017.
32. E. Sahraei, J. Campbell, and T. Wierzbicki, "Modeling and short circuit detection of 18650 Li-ion cells under mechanical abuse conditions," *Journal of Power Sources*, vol. 220, pp. 360-372, 2012. https://doi.org/10.1016/j.jpowsour.2012.07.057
33. G. R. Johnson, "A constitutive model and data for materials subjected to large strains, high strain rates, and high temperatures," *Proc. 7th Inf. Sympo. Ballistics*, pp. 541-547, 1983.
34. G. R. Johnson and W. H. Cook, "Fracture characteristics of three metals subjected to various strains, strain rates, temperatures and pressures," *Engineering fracture mechanics*, vol. 21, no. 1, pp. 31-48, 1985. https://doi.org/10.1016/0013-7944(85)90052-9
35. M. Rodriguez-Millan, D. Garcia-Gonzalez, A. Rusinek, and A. Arias, "Influence of stress state on the mechanical impact and deformation behaviors of aluminum alloys," *Metals*, vol. 8, no. 7, p. 520, 2018. https://doi.org/10.3390/met8070520
36. D. Al Galib and A. Limam, "Experimental and numerical investigation of static and dynamic axial crushing of circular aluminum tubes," *Thin-Walled Structures*, vol. 42, no. 8, pp. 1103-1137, 2004. https://doi.org/10.1016/j.tws.2004.03.001
37. Y. Xia, T. Wierzbicki, E. Sahraei, and X. Zhang, "Damage of cells and battery packs due to ground impact," *Journal of Power Sources*, vol. 267, pp. 78-97, 2014. https://doi.org/10.1016/j.jpowsour.2014.05.078
38. Gupta, S. K. (2022). Smart Grid System in India. In Indian Journal of Energy and Energy Resources (Vol. 1, Issue 4, pp. 5–6). https://doi.org/10.54105/ijeer.C1018.081422
39. Dhrawadkar, S., Dani, U. H., Harmalkar, S., & Joshi, A. (2020). Design and Simulation of Electric Vehicle. In International Journal of Recent Technology and Engineering (IJRTE) (Vol. 9, Issue 4, pp. 131–133). https://doi.org/10.35940/ijrte.C4303.119420
40. Koli, H., & Chawla, Prof. M. P. S. (2022). Comparative Study of Electric Vehicle Battery Systems with Lithium-Ion and Solid State Batteries. In International Journal of Emerging Science and Engineering (Vol. 10, Issue 10, pp. 1–6). https://doi.org/10.35940/ijese.I2540.09101022

AUTHORS PROFILE

Mr. Mizanur Rahman, the author has completed a BEng (Hons) in mechanical engineering and gained valuable insights into the intricacies of mechanical systems. His diverse professional background includes roles as a real estate salesperson at New Foil Real Estate and a vehicle mechanic at Al Doha Garage, both in Dubai. Additionally, I have served as a Junior Engineer at Motec Middle East, where I honed my engineering skills. His other areas of specialization include Computational Fluid Dynamics, Automotive, Finite Element Analysis, and 3D printing. This unique blend of experiences has equipped me with a holistic understanding of mechanical engineering principles and their real-world applications.

Mr. Mahendher Marri, the author completed a BEng (Hons) in mechanical engineering and has a diverse field background. As a Mechanical Engineering Specialist at Yamaha Motors in India, my understanding of engineering principles and their real-world applications. Later, I joined Heriot-Watt University as a Research and Teaching Assistant, where I honed my skills in academia and research. I then ventured into the industry as a Technical Support Specialist at Clean Tech in Dubai, gaining practical experience in troubleshooting and problem-solving. My research interests encompass Heat Transfer, Finite Element Analysis, Tribology, 3D printing, and Artificial Neural Networks.

Mr. Abel Varghese, the author has completed a BEng (Hons) in Mechanical Engineering and a postgraduate Diploma in Strategic Management and Leadership from Heriot-Watt University - United Arab Emirates. He represents World of Wonders Real Estate Development as a lead mechanical engineer in the United Arab Emirates. His diverse professional background includes roles as a technical advisor at Devmark and Sobha Reality, both in Dubai. His other areas of specialization include Heat Transfer, Additive Manufacturing, Tribology, 3D printing, Control systems, and Artificial Neural Networks.